ELSEVIER

Polymer 43 (2002) 5483–5491

polymer

www.elsevier.com/locate/polymer

Influence of clay exfoliation on the physical properties of montmorillonite/polyethylene composites

T.G. Gopakumar, J.A. Lee, M. Kontopoulou*, J.S. Parent

Department of Chemical Engineering, Queen's University, Kingston, Ont., Canada K7L 3N6

Received 2 April 2002; received in revised form 17 June 2002; accepted 19 June 2002

Abstract

Melt compounding was used to prepare conventional composites of montmorillonite clay and polyethylene (PE) as well as nanocomposites of exfoliated montmorillonite platelets dispersed in a maleated polyethylene (PE-*g*-MAn) matrix. The extent of clay platelet exfoliation in the PE-*g*-MAn nanocomposites was confirmed by X-ray diffraction and resulted in a significant reduction of the degree of crystallinity and increased polymer crystallization rates. Studies of non-isothermal crystallization kinetics suggested that the exfoliated clay promotes heterogeneous nucleation and two-dimensional crystallite growth.

PE/clay composites behaved in a similar manner as conventional macrocomposites, exhibiting modest increases in their rheological properties and Young's modulus. Conversely, the nanoscale dimensions of the dispersed clay platelets in the nanocomposites led to significantly increased viscous and elastic properties and improved stiffness. This was attributed to the high surface area between the polymer matrix and the exfoliated clay, which resulted in enhanced phase adhesion. © 2002 Published by Elsevier Science Ltd.

Keywords: Nanocomposite; Polyethylene; Clay

1. Introduction

The combination of clays and functional polymers interacting at the atomic level constitutes the basis for preparing an important class of inorganic–organic nanostructured materials [1–5]. Polymer-layered silicate nanocomposites containing low levels of exfoliated clays such as montmorillonite and vermiculite have a structure consisting of platelets with at least one dimension in the nanometre range. The platelet aspect ratio exceeds 300, giving rise to a high degree of polymer–clay surface interaction which results in barrier and mechanical properties that are far superior to those of the base material [1].

The preparation of nanocomposites requires extensive delamination of the layered clay structure and complete dispersal of the resulting platelets throughout the polymer matrix. Nanocomposite synthesis by conventional polymer processing operations therefore requires strong interfacial interaction between the polymer matrix and the clay in order to generate shear forces of sufficient strength. This is readily achieved with high surface energy polymers such as polyamides, where polarity and hydrogen-bonding capacity generates considerable adhesion between the polymer and clay phases. However, low-energy materials such as polyethylene and polypropylene interact only weakly with mineral surfaces, making the synthesis of polyolefin nanocomposites by melt compounding considerably more difficult [6].

Interest in polyolefin nanocomposites has emerged due to their promise of improved performance in packaging and engineering applications [6–10]. Chemical modification of these resins, in particular the grafting of pendant anhydride groups, has been used successfully to overcome problems associated with poor phase adhesion in polyolefin/clay systems [7–10]. The objective of this work was to characterize the influence of exfoliated montmorillonite on the tensile, rheological and crystallization properties of polyethylene. The extent of this influence was determined by comparison of exfoliated nanocomposites to conventional polyethylene/montmorillonite composites.

2. Experimental

2.1. Materials

Two montmorillonite clays were used as received;

* Corresponding author. Tel.: +1-613-533-3079; fax: +1-613-533-6637.
E-mail address: kontop@chee.queensu.ca (M. Kontopoulou).

0032-3861/01/$ - see front matter © 2002 Published by Elsevier Science Ltd.
PII: S0032-3861(02)00403-2

Cloisite Na + was an unexchanged material supplied by Southern Clay Inc. (Gonzales, Texas), while Nanomer® I.44PA was supplied by Nanocor Inc. (Arlington Heights, Illinois) was an ion-exchanged clay with a dimethyldialkylammonium halide (70% C_{18}, 26% C_{16} and 4% C_{14}). High density polyethylene (PE, Sclair® 2907, Nova Chemicals, MFI = 4.9) and graft-modified polyethylene containing approximately 1 wt% of maleic anhydride (PE-*g*-MAn, Fusabond® M611-25, DuPont Canada, MFI = 9.6) were used without purification.

2.2. Composite preparation

All composites were prepared by melt compounding of master batches that were premixed by dry-blending in a tumble mixer for 10 min. A Haake PolyLab torque rheometer, connected to a Rheomix 610p mixing chamber equipped with roller rotors, was operated at 190 °C, 60 rpm with a 70% fill factor for 7 min.

2.3. X-ray diffraction

The extent of clay exfoliation in the composites was determined by X-ray diffraction (XRD) using a Scintag XDS 2000 diffractometer (Cu Kα radiation $\lambda = 1.5406$ Å, generator voltage = 45 kV, current = 40 μA). Samples were pressed films approximately 400 μm thick and were scanned in 2θ ranges from 0.5 to 40° at a rate of 1°/min. Measurements were recorded at every 0.03°. For comparative purposes, the XRD patterns were represented in terms of relative intensities; the intensity of the strongest reflection was arbitrarily assigned a value of 100.

2.4. Rheological characterization

Samples for rheological characterization were disks of 25 mm diameter and 2 mm thickness that were prepared by compression moulding at 180 °C. The elastic modulus (G'), loss modulus (G'') and complex viscosity (η^*) were measured using a Reologica ViscoTech instrument as a function of the angular frequency (ω) from 0.04 to 188.50 rad/s. The rheometer was operated at 170 ± 0.1 °C in the oscillatory mode with parallel plate fixtures 20 mm in diameter and at a gap of 1.5 mm. All measurements were carried out under nitrogen to limit polymer degradation or moisture absorption. Strain sweeps were performed to verify that the measurements were within the linear viscoelastic regime. Three measurements for each composite composition were performed.

2.5. Tensile properties

A Monsanto T-10 operating at a crosshead speed of 10 mm/min at room temperature was used to determine tensile properties of the composites according to ASTM D638. Samples were prepared by compression moulding sheets 1.5 mm thick at 150 °C, from which test specimens were cut using a type M-III die. Five measurements per composite were taken to estimate the precision of reported data.

2.6. Crystallization behaviour of PE-g-MAn/clay composites

Crystallization properties were studied by using a Seiko series differential scanning calorimeter (DSC). Samples were heated from 50 to 180 °C at a rate of 10 °C/min under a nitrogen atmosphere and held for 10 min to destroy any residual nuclei before cooling at the desired rate (2.5, 5, 10, and 20 °C/min). The degree of crystallinity (corrected for clay content) was determined by integration of the DSC exotherm, from which the relative crystallinity, X, could be calculated as a function of temperature [11,12].

3. Results

Three types of structures may be obtained by melt compounding of montmorillonite clays and polyolefins: (1) delaminated nanocomposites in which the silicate layers are exfoliated into nanoscale platelets and dispersed in a continuous polymer matrix, (2) conventional composites in which micronscale clay particles are dispersed without exfoliation, and (3) partially exfoliated composites containing both delaminated and layered clay. In Sections 3.1–3.6 the structure of polyethylene–clay composites is characterized along with their physical, rheological and crystallization properties.

3.1. Compounding

We have noted that a simple indicator of the extent of clay exfoliation within polyethylene is the steady-state torque recorded during melt compounding. As shown in Fig. 1, the torque recorded during the mixing of I.44PA/PE-*g*-MAn compounds was greater than that measured for pure PE-*g*-MAn. Furthermore, the steady-state torque of PE-*g*-MAn increased with increasing I.44PA content, while no effect of clay content was observed in the unmodified polymer/clay compounds (Table 1). Based on these results, it is apparent that the modification of both the polymer (maleation) and the clay (cation exchange) produced a compound of relatively high viscosity. The structure of composites produced by melt compounding was determined by XRD analysis, as reported below.

3.2. Composite structure

Fig. 2(a) shows XRD patterns for polyethylene based composites containing 5 wt% of the I.44PA clay, while Fig. 2(b) provides similar information for the Cloisite Na + clay. The substantial reduction in the intensity of the

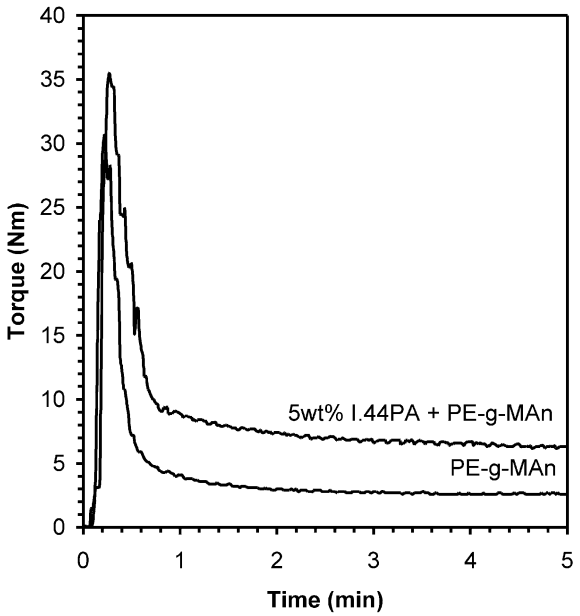

Fig. 1. Comparison of torque recorded during melt compounding for PE-*g*-MAn and 5 wt% I.44PA/PE-*g*-MAn.

diffraction peak derived from the interlayer spacing of the clay, evident in the 5 wt% I.44PA/PE-*g*-MAn composites, indicates that almost complete exfoliation of the silicate layers took place and nanocomposite structure was obtained. Intense XRD signals remained in all other polymer–clay combinations, thereby indicating that all but the PE-*g*-MAn/I.44PA system yielded conventional composites. Since no exfoliation could be achieved by using the Na + Cloisite clay, composites of this material were not pursued further.

We note that incomplete exfoliation was obtained for PE-*g*-MAn composites containing greater than 10% I.44PA clay (Fig. 3). Intense XRD signals derived from the I.44PA clay peak are apparent in these samples. The slight shift of the peak to lower angles signals the presence of a hybrid structure consisting of partially exfoliated and intercalated clay.

3.3. Rheological properties

Fig. 4 shows the relationship between complex viscosity (η^*) and frequency (ω) for I.44PA/PE-*g*-MAn

Table 1
Properties of PE, PE-*g*-MAn and their composites

Composite (compositions in wt%)	Steady-state torque (N m)	Young's modulus (MPa)	Cooling rate (°C/min)	T_c (°C)	α_c	t_p (s)	n	k ($\times 10^5$)
PE	3.5	183	2.5	117	0.50	72	2.8	0.0494
			5	115	0.49	73	3.4	0.0089
			10	113	0.48	57	3.5	0.0010
			20	110	0.48	30	3.0	0.3650
1.44PA/PE 5/95	3.5	200	2.5	123	0.50	71	2.8	0.0067
			5	120	0.50	70	2.5	0.0352
			10	116	0.49	54	2.6	0.7270
			20	114	0.49	28	2.2	0.1720
PE-*g*-MAn	2.7	169	2.5	116	0.49	104	3.2	0.0013
			5	114	0.47	63	3.6	0.0251
			10	111	0.46	41	3.3	0.0344
			20	107	0.46	28	2.9	0.7060
1.44PA/PE-*g*-MAn 3/97	3.1	207	2.5	122	0.40	53	2.2	0.7500
			5	119	0.39	41	2.2	0.8890
			10	117	0.38	30	2.4	2.0600
			20	115	0.38	18	2.3	7.0400
1.44PA/PE-*g*-MAn 5/95	3.2	220	2.5	123	0.39	52	1.7	9.6100
			5	121	0.39	37	1.6	31.500
			10	118	0.38	25	1.8	18.500
			20	116	0.37	18	1.5	196.00
1.44PA/PE-*g*-MAn 7/93	3.4	233	2.5	125	0.38	67	2.0	2.6400
			5	122	0.38	43	1.2	156.00
			10	118	0.37	32	1.2	348.00
			20	117	0.37	22	2.4	4.0200
1.44PA/PE-*g*-MAn 10/90	4.7	258	2.5	123	0.37	59	1.2	167.00
			5	121	0.36	33	1.4	72.400
			10	119	0.36	23	1.9	18.400
			20	117	0.35	15	2.2	43.700

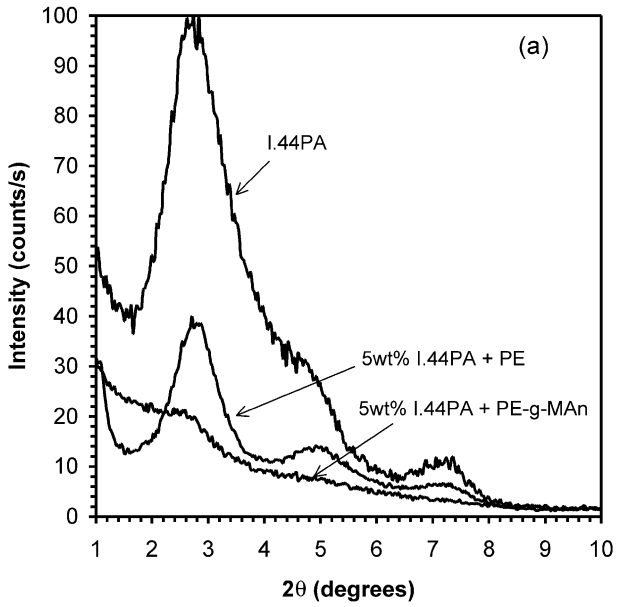

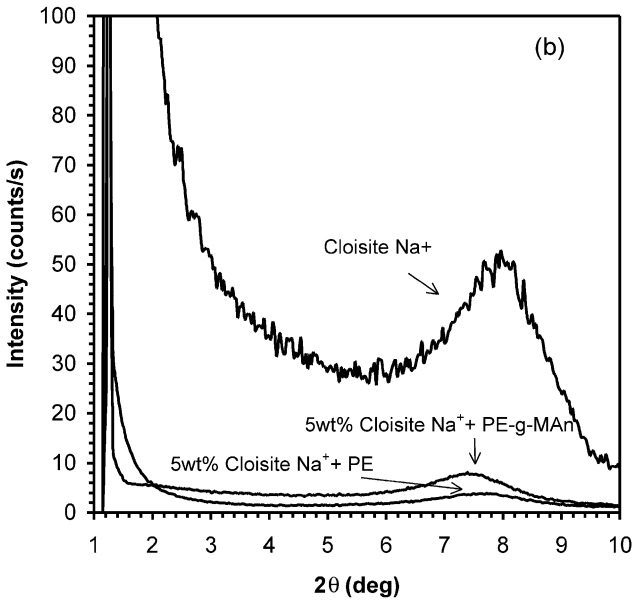

Fig. 2. (a) XRD patterns of I.44PA clay and its composites with polyethylene and PE-*g*-MAn. (b) XRD patterns of Cloisite Na + clay and its composites with polyethylene and PE-*g*-MAn.

nanocomposites of varying clay content. It is clear that η^* increased substantially at low frequencies and the Newtonian plateau disappeared as clay content increased above 5wt%. Increases of such magnitude arise in conventional composites at much higher filler loadings (above 20–30wt%) and may be attributed to the formation of weak structures that remain intact at very low frequencies [13,14].

The effect of clay exfoliation on complex viscosity is readily identified in Fig. 5. Relative to the graft-modified polyethylene system, I.44PA/PE composites demonstrated a modest increase in complex viscosity and Newtonian behaviour at low frequencies. This is the expected result

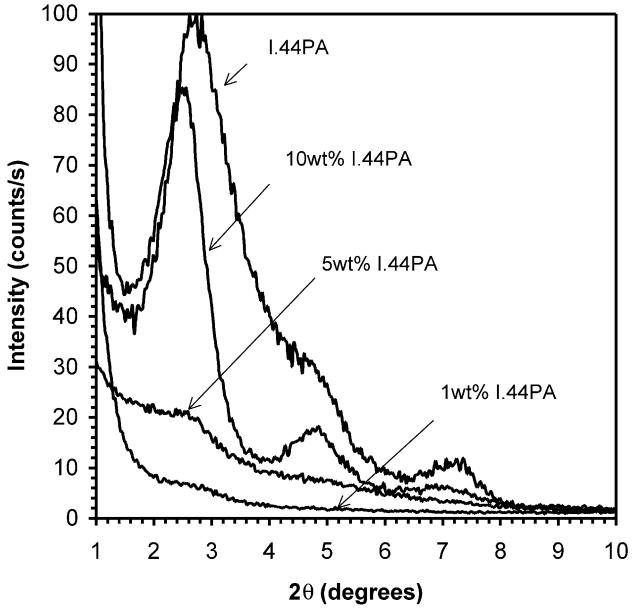

Fig. 3. XRD patterns for the I.44PA/PE-*g*-MAn system as a function of clay content.

for a macrocomposite system containing low amounts of filler [13,15].

Fig. 6 shows the relationship between the loss tangent, tan δ, and the structure of polyethylene-based composites. We noted that tan δ decreased significantly over the entire frequency range with increasing clay content in the PE-*g*-MAn nanocomposite (Fig. 6(a)), signalling a substantial deviation from terminal flow behaviour and a more elastic response as clay content increases. In contrast, tan δ decreased only marginally for the I.44PA/PE composite (Fig. 6(b)), maintaining a viscous-like response at all

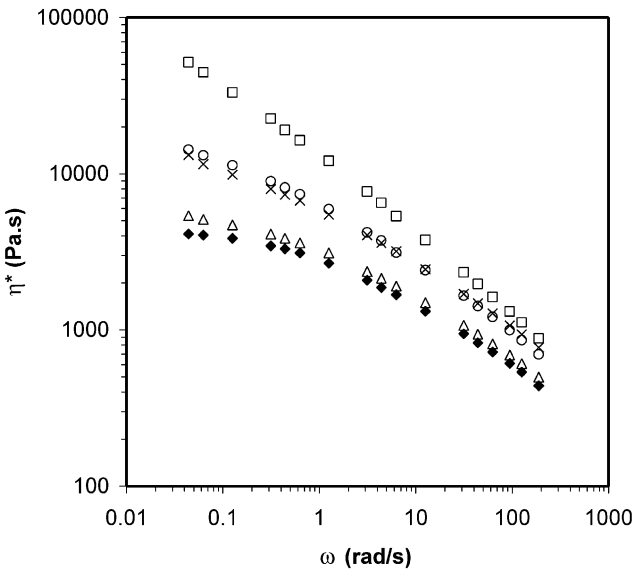

Fig. 4. Complex viscosity (η^*) as a function of frequency (ω) for the I.44PA/PE-*g*-MAn system at 170 °C: ◆ PE-*g*-MAn, △ 3 wt% I.44PA/PE-*g*-MAn, × 5 wt% I.44PA/PE-*g*-MAn, ○ 7 wt% I.44PA/PE-*g*-MAn, □ 10 wt% I.44PA/PE-*g*-MAn.

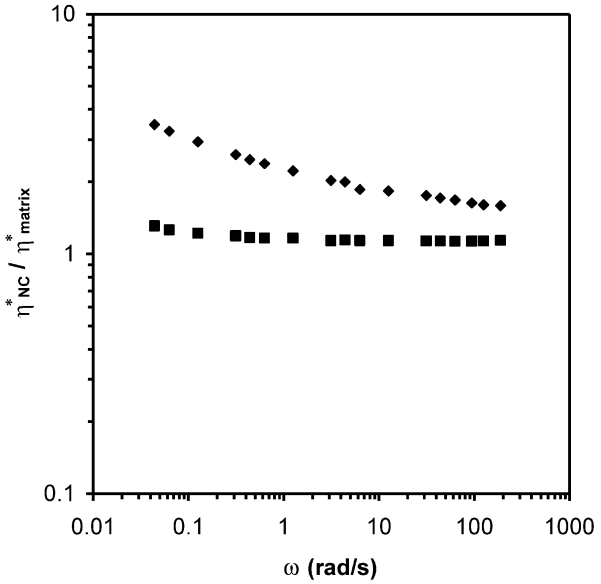

Fig. 5. Ratio of composite complex viscosity over matrix resin viscosity as a function of frequency (ω) at 170 °C: ◆ 5 wt% I.44PA/PE-*g*-MAn and ■ 5 wt% I.44PA/PE.

compositions. Previous studies [16] have shown that intercalated polystyrene nanocomposites exhibited high storage (G') and loss (G'') moduli at low frequencies, whereas exfoliated polyethylene nanocomposites showed enhanced moduli over the entire frequency range. That these reports are consistent with our findings provides further evidence of an exfoliated structure in our PE-*g*-MAn/I.44PA composites.

3.4. Mechanical properties

Table 1 lists the Young's moduli for PE, PE-*g*-MAn and their clay composites. The addition of 5 wt% I.44PA to PE resulted in a 9% increase in Young's modulus over unfilled PE. In comparison, the exfoliation of 5 wt% I.44PA in PE-*g*-MAn increased the Young's modulus by 30% while the addition of 10 wt% I.44PA clay resulted in a 53% increase over PE-*g*-MAn. However, the tensile stress at yield showed only a marginal increase, up to a maximum of 15% for the 10 wt% I.44PA clay composition. We expect the greatly enhanced interfacial area derived from exfoliation of the clay to improve the reinforcement potential of the filler. However, given that the mechanical properties of a filled system depend on two principal factors: crystallinity of the polymer matrix and the extent of filler reinforcement, the degree of crystallinity must be considered. Crystallization effects are discussed below.

3.5. Crystallinity

Representative crystallization exotherms for PE-*g*-MAn and I.44PA/PE-*g*-MAn nanocomposites are presented in

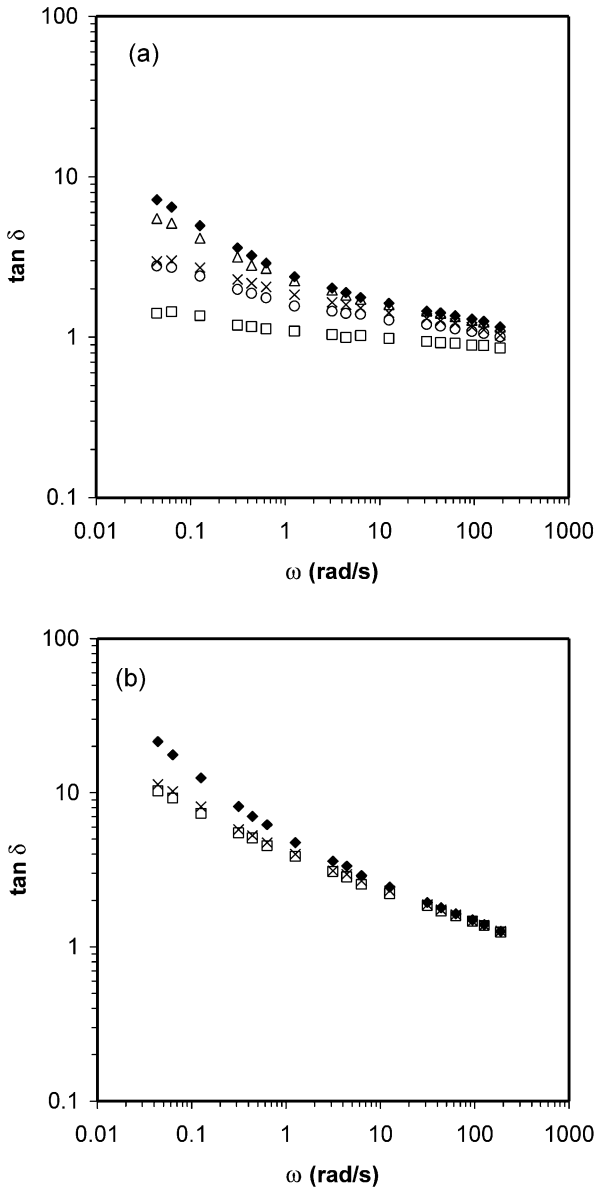

Fig. 6. (a) Loss tangent, tan δ, as a function of frequency (ω) for the I.44PA/PE-*g*-MAn system at 170 °C: ◆ PE-*g*-MAn, △ 3 wt% I.44PA/PE-*g*-MAn, × 5 wt% I.44PA/PE-*g*-MAn, ○ 7 wt% I.44PA/PE-*g*-MAn, □ 10 wt% I.44PA/PE-*g*-MAn. (b) Loss tangent, tan δ, as a function of frequency (ω) for the I.44PA/PE system at 170 °C: ◆ PE, × 5 wt% I.44PA/PE, □ 10 wt% I.44PA/PE.

Fig. 7. The depressed crystallization temperature of PE-*g*-MAn relative to PE is attributed to the influence of pendant anhydride grafts. Nevertheless, it is evident that the peak crystallization temperature (T_c) of all composites was much higher than that of PE-*g*-MAn and PE (Table 1). The observed increase of T_c with increasing clay content and decreasing cooling rate is typical for nucleation-controlled polymer crystallization [11,12].

The degree of crystallinity (α_c) in the various composites is summarized in Table 1. While α_c of PE was unaffected by the presence of I.44PA, the degree of crystallinity of PE-*g*-MAn decreased significantly upon the exfoliation of clay

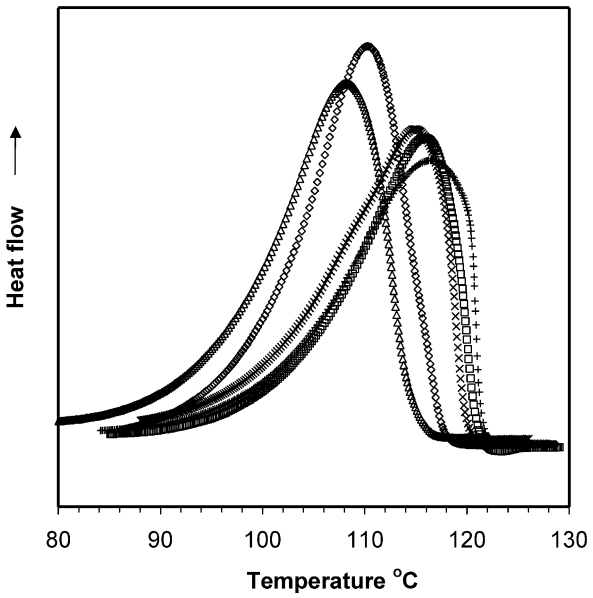

Fig. 7. DSC crystallization exotherms of PE-*g*-MAn and I.44PA/PE-*g*-MAn nanocomposites recorded at 20 °C/min: ◇ PE, △ PE-*g*-MAn, × 1 wt% I.44PA/PE-*g*-MAn, □ 3 wt% I.44PA/PE-*g*-MAn, +5 wt% I.44PA/PE-*g*-MAn.

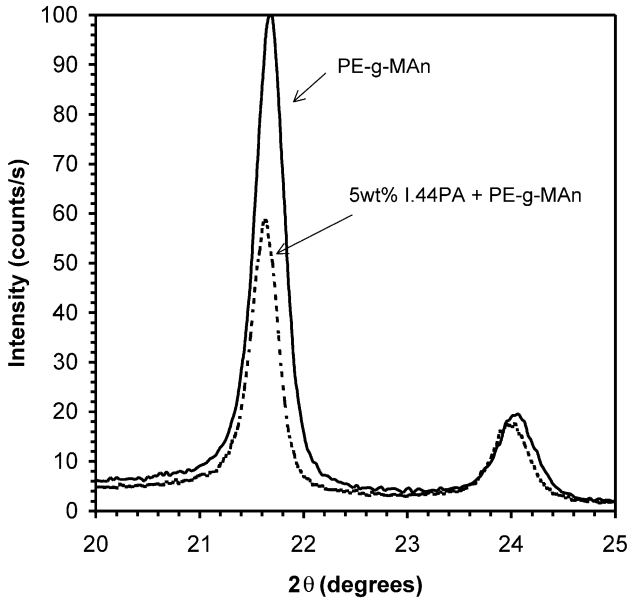

Fig. 8. XRD patterns for PE-*g*-MAn and I.44PA/PE-*g*-MAn systems depicting 110 and 200 reflections of polyethylene.

platelets. This decrease may be attributed to higher interfacial area and adhesion between the PE-*g*-MAn matrix and exfoliated clay, which would act to reduce the mobility of crystallizable chain segments. We note that reduced crystallinity in the PE-*g*-MAn based nanocomposites is expected to have a deleterious effect on mechanical properties such as tensile stress, thereby counteracting the reinforcement potential of exfoliated clay in polyolefins.

The effect of exfoliated clay on the crystalline structure of polyethylene is also obvious based on the analysis of the XRD diffraction patterns. A substantial reduction in the intensity of the 110 reflection (at $2\theta = 21.6°$) of PE-*g*-MAn is observed in the presence of exfoliated clay (Fig. 8), whereas the intensity of the same peak remained unaffected in the case of the conventional composite. Presence of clay, however, did not have an effect on the 200 reflection, located at $2\theta = 24.0°$.

3.6. Non-isothermal crystallization kinetics

The presence of exfoliated clay affected not only the degree of crystallinity, but also the rate of crystallization. Since most processing operations proceed under variable temperature conditions [11,12,17–24], our focus was on non-isothermal crystallization kinetics. The relative crystallinity was calculated as a function of temperature [11,12] and transformed to a time scale using the relationship $t = (T_0 - T)/\varphi$ (where T_0 is the onset temperature at crystallization time $t = 0$; T, the temperature at crystallization time t, and φ is the cooling rate) [22–24].

The crystallization time (t_p), defined as the period from the onset of crystallization time ($t = 0$) to the time corresponding to the peak crystallization temperature T_c [25], is summarized in Table 1. Given that the crystallization times of PE-*g*-MAn nanocomposites were reduced significantly compared to pure PE-*g*-MAn, it is evident that the crystallization rate is greatly enhanced in the presence of exfoliated clay.

While the empirical Avrami equation ($X(t) = 1 - \exp(-kt^n)$) [26] was developed to describe isothermal crystallization kinetics, it has also been used to describe non-isothermal processes. In this case, the model parameters n and k take on a different meaning given the temperature gradient applied during testing. These temperature changes ultimately affect the rates of nuclei formation and spherulite growth. Nevertheless, values of n and k have been used successfully to gain further insight into the kinetics of non-isothermal crystallization [22–24].

Representative double-logarithmic plots of $-\ln(1 - X(t))$ versus time for PE-*g*-MAn and 5 wt% I.44PA/PE-*g*-MAn samples are shown in Fig. 9. It is clear that the experimental data are represented by the Avrami equation for only the early stages of crystallization. The Avrami equation is not applicable in the late stages, where secondary nucleation takes place [22–25,27–29].

The non-isothermal crystallization parameters k and n fitted to the kinetic data are listed in Table 1. The Avrami exponent of PE and PE-*g*-MAn is close to 3, which indicates that spherulite growth likely occurred with homogeneous nucleation. This value of n is within the range of values for high-density PE reported in the literature [25,27–29]. The values of n for I.44PA/PE-*g*-MAn nanocomposites were lower than those of the PE and PE-*g*-MAn at the same cooling rate. In the case of I.44PA/PE-*g*-MAn nanocomposites, the Avrami exponent was between 1 and 2, suggesting

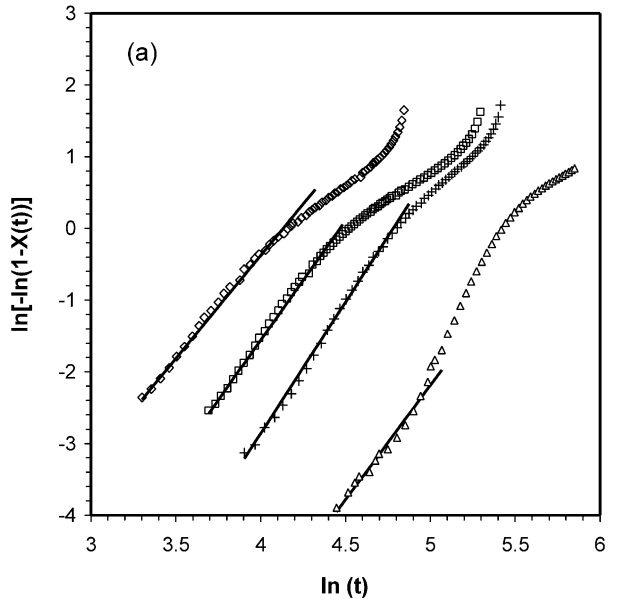

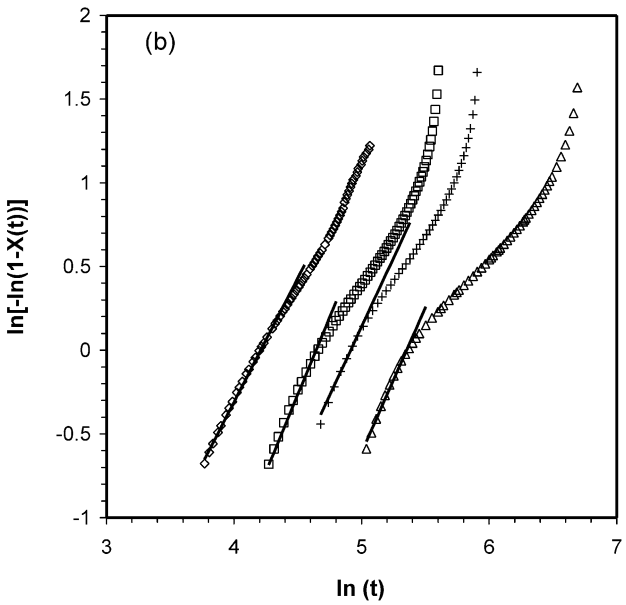

Fig. 9. Avrami plots of $\ln(-\ln[1 - X(t)])$ versus $\ln(t)$ for crystallization of (a) PE-*g*-MAn and (b) 5 wt% I.44PA/PE-*g*-MAn nanocomposites: △ 2.5 °C/min, +5 °C/min, □ 10 °C/min, ◇ 20 °C/min.

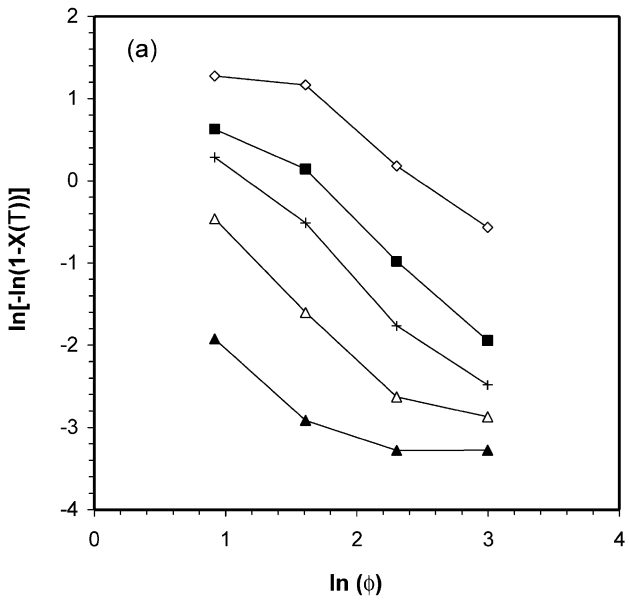

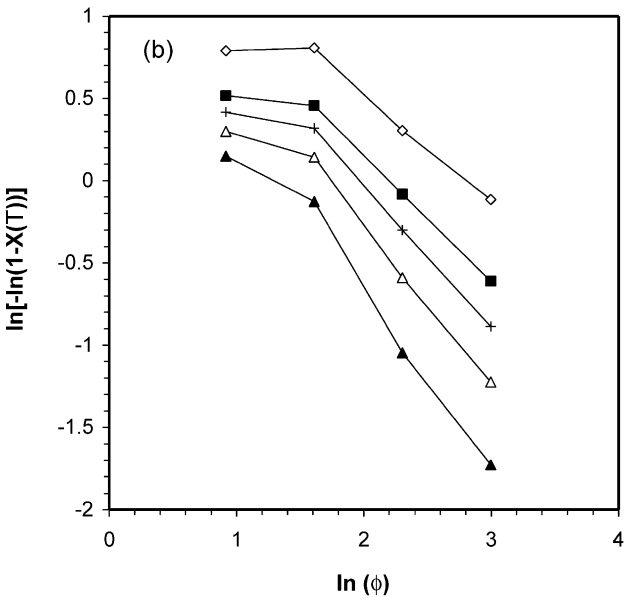

Fig. 10. Ozawa plots of $\ln(-\ln[1 - X(T)])$ versus $\ln(\phi)$ for crystallization of (a) PE-*g*-MAn and (b) 5 wt% I.44PA/PE-*g*-MAn nanocomposites: ◇ 106 °C, ■ 112 °C, +114 °C, △ 116 °C, ▲ 118 °C (lines drawn to guide the eye).

that the nucleated process led to two-dimensional, heterogeneous growth. It is possible that anisotropic clay platelets act as nuclei for the initial nucleation and subsequent growth of crystallites.

The Avrami crystallization rate constant (k) is also affected by the concentration of exfoliated clay, as we observed a pronounced increase with increasing clay content. Based on Mandelkern's analysis [11], we therefore suggest that the crystallization of PE-*g*-MAn involves homogeneous nucleation, whereas the nanocomposites crystallize through heterogeneous nucleation followed by two-dimensional, diffusion-controlled growth. It can be concluded that the type of nucleation and geometry of crystal growth of PE markedly change in the presence of exfoliated clay. Similar observations of polymer crystallization in the presence of exfoliated clays have been reported [21–23].

Non-isothermal crystallization kinetics can be described by using the extension of the Avrami theory proposed by Ozawa [30]

$$X(T) = 1 - \exp\left(-\frac{k}{\phi^n}\right) \quad (1)$$

where $X(T)$ is the relative crystallinity as a function of

temperature; k, the Ozawa crystallization rate constant; n, the Ozawa exponent (similar to the Avrami exponent) and ϕ is the cooling rate.

Double logarithmic plots of $\ln[-(1 - X(T))]$ versus ϕ for fixed temperatures, are shown in Fig. 10(a) and (b) for PE-*g*-MA and 5wt%1.44PA/PE-*g*-MAn nanocomposites, respectively. These plots do not represent straight lines, which means that the Ozawa equation was not successful in describing the non-isothermal crystallization behaviour of the present materials. This is probably due to factors such as secondary crystallization of polyethylene, dependence of lamellar thickness on crystallization temperature and variation of Avrami's exponent with crystallization temperature neglected in the theory of Ozawa [31].

4. Discussion

Based upon our XRD analysis, melt compounding experiments and rheological characterization, it can be concluded that two conditions are required to produce the intensity of surface interactions required to exfoliate and disperse the clay in a polyolefin matrix. Firstly, the montmorillonite clay must be ion-exchanged to reduce the cohesive forces between clay platelets. Secondly, the polyolefin must be chemically modified to improve adhesion between the polymer matrix and clay filler. The origin of these surface interactions is not presently understood. One possibility is that polar anhydride functionality promotes dipole and/or hydrogen bonding between the filler and the polyolefin, thus leading to improved dispersion of the clay in the polymer matrix.

Exfoliated clay platelets have a flexible, sheet-type structure whose thickness is in the order of 1 nm and lateral dimensions (length and width) range from several hundred nanometres to a few microns. On the other hand, conventional composites contain clay particles with micronscale dimensions. Therefore, the principal difference between the nanocomposites and conventional composites examined in this work is the nanoscale dimensions of the filler in the former and the resulting interfacial area per unit volume. Consequently, thermodynamics and kinetics of polymer chain conformations should be affected to the greatest extent in a nanocomposite. We, therefore, suggest that high interfacial area, leading to enhanced interaction between anisotropic clay platelets and maleated polyethylene, is the cause for the notable differences in the physical, mechanical and melt-phase properties between nanocomposites and conventional composites. The observed improvements in Young's modulus provide further evidence of the enhanced reinforcement potential of the nanocomposites.

The type of nucleation and geometry of crystal growth of polyethylene are also affected in the presence of exfoliated clay. The nanoscale particulates act as nucleating agents, facilitating the heterogeneous crystallization process. The fact that the particulates are well dispersed leads to an increased number of sites available for nucleation, therefore enhancing the crystallization rate and altering the kinetics and geometry of crystal growth. Due to restrictions in polymer chain mobility through association with exfoliated platelets, a significant reduction in the degree of crystallinity is observed, which can negate the reinforcement capability of the nanoclays.

5. Conclusions

Chemical modification of both the polyolefin and montmorillonite clay is necessary to generate polyethylene nanocomposites by melt compounding. The resulting rheological, thermal and mechanical properties are sensitive to the composite structure and clay content. In the presence of completely exfoliated clay, the nanoscale dispersed clay layers act as nucleating agents, resulting in enhanced polymer crystallization rate, increased crystallization temperature and reduced the degree of crystallinity. A notable reduction in the Avrami exponents for the nanocomposites suggests that exfoliated clay results in heterogeneous nucleation and two-dimensional crystallite growth. Significantly higher viscosity, elasticity and Young's modulus observed for the nanocomposites provides evidence of improved surface area/adhesion between the polymer matrix and the exfoliated clay.

Acknowledgments

This work has been supported financially by Natural Sciences and Engineering Research Council (NSERC) and the Centre for Automotive Materials and Manufacturing (CAMM). The authors wish to thank Nanocor Inc. for supplying clay samples, and Mr Doug Pfeiffer of Alcan for assistance with XRD analysis.

References

[1] Pinnavaia TJ, Beall GW, editors. Polymer–clay nanocomposites. New York: Wiley; 2001.
[2] Kawasumi M, Hasegawa N, Kato M, Usuki A, Okada A. Macromolecules 1997;30:6333.
[3] Heinemann J, Reichert P, Thomann R, Mulhaupt R. Macromol Rapid Commun 1999;20:423.
[4] Oya A, Kurokawa Y. J Mater Sci 2000;35:1045.
[5] Giannelis EP. Adv Mater 1996;8:29.
[6] Guoqiang Q, Cho JW, Lan T. Proceedings of Polyolefins 2001, Houston, TX.
[7] Hambir S, Bulakh N, Kodgire P, Kalaonkar R, Jog JP. J Appl Polym Sci 2001;39:446.
[8] Galgali G, Ramesh C, Lele A. Macromolecules 2001;34:852.
[9] Rong MZ, Zhang MQ, Zheng YX, Zeng HM, Walter R, Friedrich K. Polymer 2001;42:167.

[10] Wang KH, Choi MH, Koo CM, Choi YS, Chung IJ. Polymer 2001;42:9819.
[11] Mandelkern L. Crystallization of polymers. New York: McGraw-Hill; 1964.
[12] Wunderlich B. Macromolecular physics. New York: Academic Press; 1973.
[13] Khan SA, Prud'homme RK. Rev Chem Engng 1987;4:205.
[14] Faulkner DL, Schmidt LR. Polym Engng Sci 1977;17:657.
[15] Poslinski AJ, Ryan ME, Gupta RK, Seshadri SG, Frechette FJ. J Rheol 1988;32:703.
[16] Lim YT, Park OO. Rheol Acta 2001;40:220.
[17] Di Lorenzo ML, Silvestre C. Prog Polym Sci 1999;24:917.
[18] Gopakumar TG, Ghadage RS, Ponrathnam S, Rajan CR. Polymer 1997;38:2209.
[19] Day M, Suprunchuk T, Cooney JD, Wilkes DM. J Appl Polym Sci 1988;36:1097.
[20] Hong SM, Kim BC, Kim KU, Chung IJ. J Polym 1992;24:727.
[21] Tseng CR, Lee HY, Chang FC. J Polym Sci, Part B: Polym Phys 2001;39:2097.
[22] Xu W, Ge M, He PJ. Appl Polym Sci 2001;82:2281.
[23] Xu W, Ge M, He PJ. J Polym Sci, Part B: Polym Phys 2002;40:408.
[24] Supaphol P. J Appl Polym Sci 2000;78:338.
[25] Gupta AK, Rana SK, Deopura BL. J Appl Polym Sci 1994;51:231.
[26] Avrami MJ. Chem Phys 1939;7:1130.
[27] Hay JN, Perzekop ZJ. J Polym Sci, Polym Phys Ed 1978;16:81.
[28] Hay JN, Mills PJ. Polymer 1982;23:1380.
[29] Rabesiaka J, Kovacs AJ. J Appl Phys 1961;32:2314.
[30] Ozawa T. Polymer 1971;12:150.
[31] Eder M, Wlochowicz A. Polymer 1983;24:1593.